# Exploiting Chaos to Suppress Spurious Tones in General Double-Loop ΣΔ Modulators

Søren Hein, *Member, IEEE*

***Abstract*— Conventional ΣΔ modulators are operated exclusively in the nonchaotic regime in which the internal integrators are stable. Theoretical interest in chaotic ΣΔ modulators recently arose, mainly because the circuits are simple and strongly nonlinear systems with rich behavior, not unlike Chua's circuit [1], [2]. It has since been recognized that the application of conventional ΣΔ modulators to A/D and D/A conversion may be haunted by spurious "tones" in the output, and it has been proposed to use chaotic modulators to overcome that problem. This paper employs a semi-analytical technique to solve the design problem for general chaotic double-loop modulators with constant inputs. Using the results, optimized scaling factors are easily found for given integrator pole locations, such that an approximate performance measure is maximized subject to bounds on internal state variables. The clarification of this explicit tradeoff between tone rejection through chaos, system stability, and practical performance may help to overcome some understandable skepticism in the community of ΣΔ designers.**

## I. Introduction

ΣΔ MODULATION is by now established as an important technique for analog-to-digital (A/D) and digital-to-analog (D/A) conversion for relatively low-bandwidth applications such as speech and audio [3]. As ΣΔ modulators for A/D conversion require few, simple and relatively low-precision analog components, they are well suited to on-chip VLSI implementation. Their advantages come at the expense of sampling rates much higher than the Nyquist rate.

The original and simplest ΣΔ modulator for A/D conversion is the single-loop modulator [4] shown in Fig. 1. It consists of a 1-b quantizer $Q$ specified by

$$Q(U) = \begin{cases} +1 & \text{for } U > 0 \\ -1 & \text{for } U \le 0, \end{cases}$$

and embedded in a negative feedback loop which also contains a discrete-time integrator. The analog input sequence is oversampled and converted to a binary output sequence, which upon low-pass filtering and decimation approximates the analog input. When the input equals a constant $X$ and the integrator is ideal, the circuit is essentially an implementation of the well-known circle map [5]. In practice, the integrator is often leaky due to finite operational amplifier (op-amp) gain, that is, the state equation is of the form

$$U_n = \alpha U_{n-1} + X - Q(U_{n-1}),$$

Manuscript received May 25, 1993; revised June 4, 1993. This paper was recommended by Associate Editor L. Chua.

S. Hein is with Siemens AG, Corporate Research and Development, München, Germany.

IEEE Log Number 9211624.

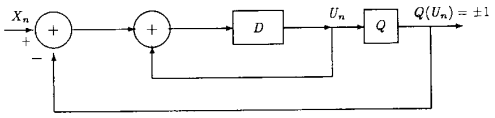


Fig. 1. Discrete-time model of the single-loop ΣΔ modulator. $D$ represents a delay element.

where the constant $\alpha$ is less than 1, as $\alpha \approx 1 - 1/A$ for an op-amp gain of $A \gg 1$. The case of leaky integration was studied from a dynamical-systems point of view by Feely and Chua [6]. The integrator constant $\alpha$ can however also be made greater than one at the expense of some additional circuitry; this case was investigated by the same authors in [7]. It was shown that for $\alpha > 1$, the single-loop modulator can behave chaotically, and a number of interesting characteristics were uncovered.

In parallel with the cited work, the circuit design community arrived at the conclusion that ΣΔ modulators are prone to exhibit spurious "tones" in the filtered modulator output, that is, sinusoidal oscillations which are introduced by the circuit nonlinearity and which would be audible in an audio application—hence, the name "tones." The tones are related to limit cycle behavior in the modulators. Although the problem had been known for some time [8] and had been analyzed thoroughly in the case of the single-loop modulator [9], the message was brought home particularly clearly at the ISCAS'92 conference in [10]. As a consequence, it was proposed to move the integrator poles outside of the unit circle and deliberately make the modulators chaotic in order to "randomize" the internal state variables, reduce long-term predictability and break up simple oscillations. Such proposals can be found in [11]–[14]. Introducing chaos is an attractive alternative to dithering [12], whose properties are somewhat incompletely understood [10], and which may require more circuitry.

The present work is concerned with the general double-loop ΣΔ modulator shown in Fig. 2, which contains as parameters the scaling factors ($g$, $G$, $b$, $B$) as well as the integrator poles ($\alpha$, $\beta$) and which has constant input $X$. This modulator is a generalization of the original double-loop modulator proposed by Candy [15] to provide a better trade-off than the single-loop modulator between the oversampling ratio (OSR) of the input relative to the Nyquist rate on one side, and the signal-to-noise ratio (SNR) in approximating the input on the other side. The double-loop modulator has shown to be a good all-round circuit on its own or as a building block in cascaded configurations. The general modulator was first analyzed in

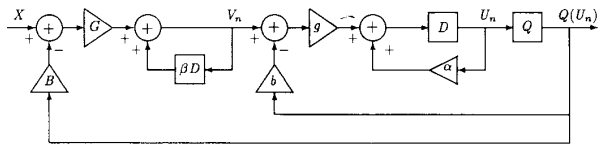


Fig. 2. Discrete-time model of the double-loop ΣΔ encoder.

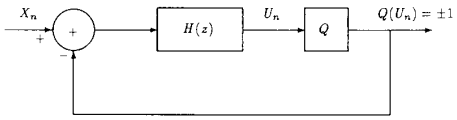


Fig. 3. Discrete-time model of the interpolative ΣΔ modulator.

[14], [16], and [17] for the special case of perfect integrators ($\alpha = \beta = 1$) and constant inputs. Independent work using essentially the same approach was presented by Wang in [18].[1] More recently, Pinault and Lopresti [19] used related techniques specifically for the standard Candy modulator with a finite sum of sinusoids as its input. Motamed *et al.* [13] considered the Candy modulator with arbitrary integrator poles and constant inputs, mostly in qualitative or approximate terms. The present work uses a semi-analytical version of the analytical technique proposed in [14], [16], and [17] to quantify the tradeoff between system stability, performance, and tone persistence. The main contributions are the extension to the chaotic regime and the resulting explicit design tables.

The paper is organized as follows. Section II discusses the specific aspects of ΣΔ modulators that are brought out by the operation in the chaotic regime. Section III summarizes and generalizes the idea behind the bounding technique that is also the basis of previous work [14], [16], [17], whereas Section IV shows how to employ the bounding technique for chaotic modulator design. Section V presents the design results in the form of a table. Finally, Section VI contains conclusions.

## II. Chaotic Regime

Chaotic behavior is characterized by state-space trajectories that locally diverge exponentially from one another, yet globally remain within a bounded region [20]. ΣΔ modulators with open-loop poles outside of the unit circle have the potential to exhibit chaotic behavior, because differences in initial integrator states are magnified exponentially. For the single-loop and double-loop modulators, the open-loop poles are identical to the integrator poles. For more general modulators like the interpolative modulator in Fig. 3, the open-loop poles are the poles of the discrete-time filter $H(z)$. For convenience, we will also refer to the poles of $H(z)$ as integrator poles regardless of the implementation of $H(z)$.

When the integrator poles are outside of the unit circle, the state-space trajectories are unstable. However, it is sadly easy to construct ΣΔ modulators which are unstable systems, that is, modulators whose state variable values tend towards infinity. To obtain chaotic behavior, the 1-b quantizer must act to fold the diverging trajectories back into a bounded region of state space. Following these two considerations, a ΣΔ modulator is chaotic if at least one integrator pole is outside of the unit circle,[2] and the system has bounded state variables for a given class of inputs and initial states. On the other hand, any ΣΔ modulator with all its poles inside of the unit circle is non-chaotic. Modulators with poles on the unit circle are structurally unstable [21] in the sense that arbitrarily small pole perturbations change the type of dynamics associated with the poles in question. In the case of chaotic behavior, the dimension of the system is simply the order of the modulator filter, and the discrete-time Lyapunov exponents are determined by the integrator poles [12]–[14].

It is easily shown that for any modulator with at least one integrator pole outside of the unit circle, there exist initial state values which lead to unbounded state variable values. Assuming simple poles, we need only consider the integrator $I$ with the largest pole modulus, and make the initial state of $I$ so large that the contributions from other circuit sources can never increase enough to change the sign of the output of $I$. The output of $I$ will then eventually be dominated by the exponential growth associated with its own pole. This prescription can be generalized to multiple poles. It follows that no modulator is chaotic for all possible initial integrator states.

This negative result suggests that the design of chaotic modulators must concentrate on state-space properties, and must aim to guarantee that state variable values giving rise to system instability cannot occur. In general, such a task appears extremely difficult, although the simple single-loop modulator can be thoroughly analyzed [21]. This paper uses semi-analytical bounding techniques to attack the design problem for the general double-loop modulator.

By way of motivation, let us demonstrate the effect of moving into the chaotic regime. Fig. 4(a) shows 1500 samples of filtered output from the standard Candy double-loop modulator defined by $\alpha = \beta = 1$, $g = G = b = B = 1$ with a constant input of $X = 0.1$. Fig. 4(b) uses the same set-up, except that the integrator poles have been moved to $\alpha = \beta = 1.01$. In both cases, the binary modulator output has been filtered with a sixth order Butterworth lowpass filter whose baseband corresponds to an oversampling ratio of OSR $= 32$. An infinite impulse response (IIR) filter was preferred over a finite impulse response (FIR) one for simplicity and reaction time. Note that the fast Fourier transform (FFT) is an impractical tool for tone analysis for two reasons: First, tones may be difficult or impossible to notice in the output spectrum [10], and second, the interplay between tone persistence and FFT length would complicate the interpretation of results for chaotic modulators.

In Fig. 4(a), we observe a sinusoidal oscillation or "tone" around the dc level of 0.1; the tone would be very unwelcome in an audio application. In Fig. 4(b), the phase of the tone has been efficiently randomized, such that the frequency content of the irregular oscillation is shifted and spread over a larger frequency range. When played back as an audio signal at a sampling frequency of 8192 Hz, the waveform of Fig. 4(a)

[1] Note that due to an error in the detailed proof, the numerical results presented in [18] are incorrect.

[2] Technically, the output of this integrator must also be observable.

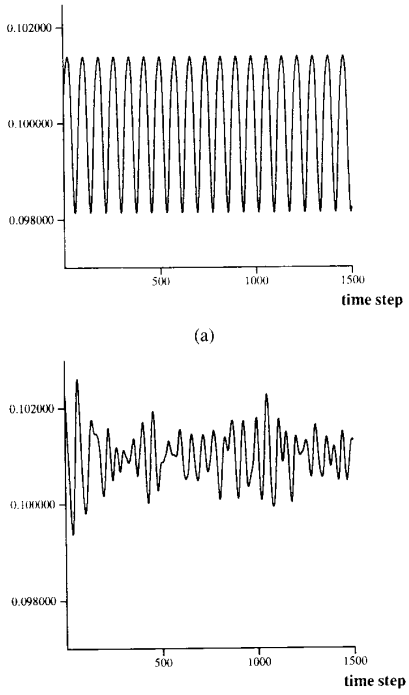


Fig. 4. Moving integrator poles outside of the unit circle suppresses tones: (a) Modulator pole moduli 1; (b) modulator pole moduli 1.01.

sounds like a tone, whereas the waveform of Fig. 4(b) is harder to hear and has practically no audible single-tone content. On the other hand, the average level of the filtered output differs more from 0.1 for the chaotic modulator than for the non-chaotic one, suggesting an SNR degradation. This design tradeoff is exploited in Section IV.

## III. Bounding Technique

The presented work is based on a semi-analytical technique for bounding the state variables $U_n$ and $V_n$ of the double-loop modulator shown in Fig. 2. The technique works only for constant inputs. Several arguments can be given in favor of limiting the focus to constant inputs [14] including the following: The oversampling of the input implies that the input is quite slowly varying, and constant inputs constitute an important special class which is a subset of any reasonable input class. Our goal is to perform a stability analysis which is more realistic than the standard bounded input bounded output (BIBO) one. Obtaining tight numerical bounds on state variables is important because the state variable voltages are limited in any practical implementation by factors such as supply voltage and op-amp output swing. If the mathematical equations describing the idealized circuit dictate a voltage exceeding the circuit capability, *clipping* or *saturation* will occur, which entails serious performance degradation. Therefore, a practical circuit must be designed, that is, scaling factors and other circuit parameters must be chosen such that clipping does not occur under normal operation. Our bounding technique [14], [16], [17] solves this problem.

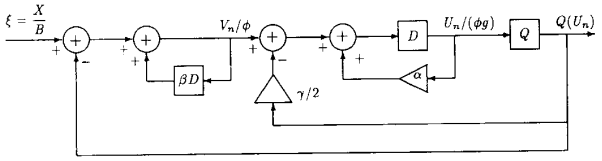


Fig. 5. Discrete-time model of the normalized double-loop ΣΔ encoder.

Our technique operates on the 2-D state space of the double-loop modulator in Fig. 2 or, equivalently, on the normalized modulator shown in Fig. 5. The connection between the two figures is specified by the equations

$$\phi = GB, \quad \gamma = \frac{2b}{GB} = \frac{2b}{\phi}, \quad \xi = \frac{X}{B}. \tag{1}$$

The original and normalized modulators are specified by the parameter sets $(g, G, b, G; X)$ and $(\gamma, \phi, g, B; \xi)$, respectively. In terms of the normalized circuit, the state equations are[3]

$$\begin{aligned} U_n &= \alpha U_{n-1} + gV_{n-1} - \frac{g\gamma\phi}{2} Q(U_{n-1}) \\ V_n &= \beta V_{n-1} + \phi\xi - \phi Q(U_n). \end{aligned} \tag{2}$$

The state space is divided into two half planes called the positive and negative half planes, depending on the value of $Q(U_n)$. Each half plane is further divided in two by a transition half-line given by

$$\alpha U_{n-1} + gV_{n-1} = a\frac{g\gamma\phi}{2} \tag{3}$$

where $a = +1$ and $-1$ for the positive and negative half planes, respectively. The transition lines and the axes delimit two triangular regions shown in Fig. 6, which we call transition regions, because an initial state $(U_n, V_n)$ in a transition region is mapped into a state $(U_{n+1}, V_{n+1})$ in the opposite half plane by (2). As long as a state trajectory stays outside of the transition regions, the state equations are linear because the quantizer output $Q(U_n)$ remains at a fixed value. For the special case of ideal integrators ($\alpha = \beta = 1$), successive state variables then fall on a parabola whose symmetry axis is parallel to the $U$ axis in state space [14], [17]. In general, however, the state trajectories in each half plane trace out a curve with no closed analytical form. The family of curves in a half plane are nested, one inside another, typically parabola-like in shape, and do not intersect. We refer to each continuous curve as a potential curve, and we associate to each curve a potential which is the largest absolute value of $U$ occurring on the curve. The potentials corresponding to the curves in the two half planes are called positive and negative potentials; note that both these potentials only assume nonnegative values.

The discrete-time system (2) is conveniently analyzed by conferring upon it the freedom to move continuously along the potential curves, so long as the trajectories remain outside of the transition regions. A half plane transition occurs when

[3] As an aside, we note that finite operational amplifier gain in the integrators can be modeled well as an effective decrease in $\alpha$ and $\beta$.

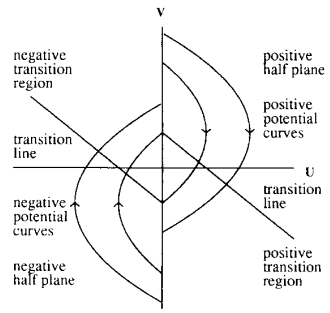


Fig. 6. Partitioning of state space into half planes and transition regions.

a potential curve reaches a transition region; we allow the system to choose any point on the current potential curve within the transition region as the discrete point from which the system changes half planes according to (2). The resulting semi-continuous (SC) system can achieve a larger range of state variable values than the underlying discrete-time (DT) system; therefore, bounds on state variables that are valid for the SC system are also valid for the DT system.

The SC system is analyzed by considering the half plane transitions. For a given positive potential, a range of negative potentials are possible as the positive potential curve in general has several intersection points with the positive transition region. We can determine upper and lower bounds on the negative potential $P_{\text{neg}}$ as a function of the originating positive potential $P_{\text{pos}}$. Similarly, when going from the negative to the positive half plane, we can determine upper and lower bounds on $P_{\text{pos}}$ as a function of the originating $P_{\text{neg}}$. In the case of ideal integrators, these calculations and all the following ones can be carried out analytically, and although the calculations are tedious and must take several special cases into account, closed form solutions exist [14], [17]. In the more general case, the bounds can be determined by numerical optimization.

The obtained bounds can next be combined to give bounds on the positive potential $P_{\text{pos2}}$ as a function of the previous positive potential $P_{\text{pos1}}$, eliminating the intermediate negative potential $P_{\text{neg}}$. Numerically, this is done by considering the range of possible $P_{\text{neg}}$ for a given $P_{\text{pos1}}$ and then finding the smallest lower bound and the greatest upper bound on $P_{\text{pos2}}$ over the possible values of $P_{\text{neg}}$. Similarly, we can obtain bounds on the negative potential $P_{\text{neg2}}$ as a function of the previous negative potential $P_{\text{neg1}}$. This leaves us with a discrete map from one positive potential to the subsequent positive potential, and similarly for the negative potential. Our bounding technique is based on the analysis of these two maps. As a representative example, Fig. 7 shows the positive potential map for the standard double loop modulator with a constant input of 0. For future reference, the figure also shows the 45° line and the square to which the potential is eventually restricted.

The goal of the analysis in [14] and [17] was to find a range of potentials $[P_A, P_B]$ for each of the positive and negative potential maps with the following four properties:

1. When $P_A \leq P_1 \leq P_B$, the greatest upper bound and the least lower bound on the subsequent potential $P_2$ lies between the same bounds. In words, the potential cannot escape the interval $[P_A, P_B]$, and the upper and lower bounds are contained in the square $[P_A, P_B]^2$.
2. When $P_1 > P_B$, the subsequent potential is smaller than $P_1$. In words, the upper bound is below the 45° line $P_2 = P_1$ for $P_1 > P_B$.
3. When $0 \leq P_1 < P_A$, the subsequent potential is greater than $P_1$. In words, the lower bound is above the 45° line for $0 \leq P_1 < P_A$.
4. When $0 \leq P_1 < P_A$, composing the potential map with itself cannot give rise to potentials lower than the starting potential $P_1$. If the upper bound $P_{\max}(P_1)$ at the starting potential $P_1$ is less than $P_B$ for all $P_1$ less than $P_A$, this property follows automatically. Otherwise, the property requires that the least lower bound over the range $[P_B, P_{\max}(P_1)]$ is greater than $P_1$, for all $P_1$ less than $P_A$.

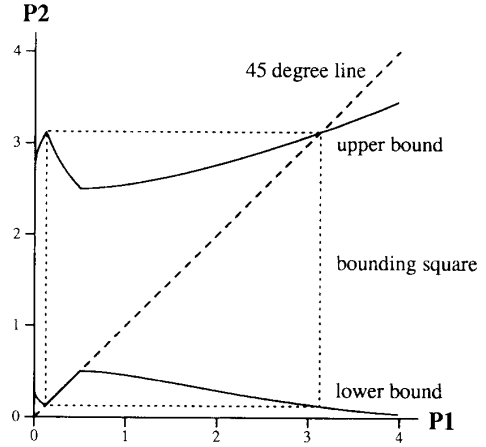


Fig. 7. Positive potential map: Upper and lower bounds.

If the range of potentials $[P_A, P_B]$ exists, it can be shown that the potential must belong to that range in steady state; we refer to this fact as the bounding theorem. If the potential starts outside of the range, the range acts as an attractor, and once the potential is inside the attracting range, the potential remains there. The value of the potential is therefore bounded in steady state. By combining the results for positive and negative potentials, an overall bound on the absolute value of the state variable $U$ is established. As the potential curves are bounded, corresponding bounds on the other state variable $V$ can be derived.

An alternative, weaker form of the bounding theorem can be obtained, which is useful for the analysis of the chaotic double-loop modulator. In the alternative form, our goal is to find a potential range $[P_A, P_B]$ and a potential $P_C$ with properties 1, 3, and 4 as above that satisfy the following as well:

1. When $P_B < P_1 \leq P_C$, the subsequent potential is below $P_1$. In words, the upper bound is below the 45° line for $P_B < P_1 \leq P_C$.
2. When $P_1 > P_C$, the subsequent potential is above $P_1$.
3. The greatest upper bound over the range $0 \leq P_1 < P_A$ is less than $P_C$.

If the constants $P_A$, $P_B$, and $P_C$ exist, potentials that start below $P_C$ will converge such that the potential is eventually restricted to the range $[P_A, P_B]$. On the other hand, potentials above $P_C$ may lead to unbounded state variables. We can thus make the limited, but nonetheless useful statement that if the state variables start out in a region specified by the bounds derived from $P_C$, the state variables are bounded. If clipping sets in between $P_B$ and $P_C$, the possibility of instability or detrimental clipping is effectively eliminated, even though the idealized mathematical system is unstable for certain initial conditions. In this case, the nonlinear clipping neutralizes the possibility of system instability introduced by making the modulator chaotic.

In the special case of perfect integration, it is shown in [14] and [17] that for $0 \leq \xi < 1$, the state variables are upper bounded by

$$\frac{8|U_n|}{\phi g} \leq \begin{cases} \frac{\left[(\gamma-1)(1-\xi)+\frac{2\gamma}{\gamma-1}\right]^2}{1-\xi} & \text{for } 1 < \gamma \leq 1+\frac{2}{1+\xi} \\ \frac{16+\gamma^2(1-\xi)^2}{1-\xi} & \text{for } 1+\frac{2}{1+\xi} < \gamma \leq f(\xi) \\ \frac{\gamma(1+\xi)+2]^2}{1+\xi} & \text{for } f(\xi) < \gamma, \end{cases} \tag{4}$$

where

$$f(\xi) = \frac{-1+\sqrt{1+2\xi\left(\frac{4}{1-\xi}-\frac{1}{1+\xi}\right)}}{\xi}, \tag{5}$$

and

$$\frac{2|V_n|}{\phi} \leq \begin{cases} \gamma\left(\xi+\frac{2}{\gamma-1}\right) & \text{for } 1 < \gamma \leq 1+\frac{2}{1+\xi} \\ (\gamma+1)\xi+3 & \text{for } 1+\frac{2}{1+\xi} < \gamma. \end{cases} \tag{6}$$

A program has been written which implements the described bounding algorithm. Although the program is conceptually straightforward, its implementation consists of about 1500 lines of C code. The program reproduces the analytical bounds in the special case of ideal integrators. The running time is on the order of minutes on a Sun SPARC-10 station, due to a number of time-consuming nested optimizations.

To illustrate the tightness of the bounds obtained with the program, Fig. 8 shows the bounds as well as actual maximum state variable values observed in 100 simulations over 10 000 samples each as a function of the constant input. The results are obtained for the optimized modulator derived in Section V with poles at $\alpha = \beta = 1.01$, and the initial states are chosen at random for each run within the region $(U, V) \in [-10, +10] \times [-2, +2]$ of state space. The figure shows that the bounds are 5–15% above the maximum observed values for $\xi_{\max}$ up to 0.6, which is the range that is mostly used in the design process. The figure thus indicates that the bounds are tight enough to be used for design.

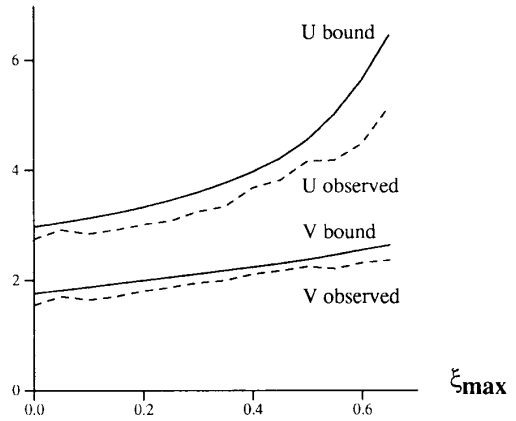


Fig. 8. Simulated maximum state variable values for the optimized modulator with poles at 1.01.

## IV. Design Tradeoffs

In Section 4.1, we derive an approximate performance measure describing the general double-loop modulator as an A/D converter. In Section 4.2, we quantify the effect of integrator poles on tone suppression. In Section 4.3, we combine our results in a design procedure that takes both SNR performance and tone suppression into account, and which optimizes system stability subject to these two competing constraints.

### 4.1. Approximate SNR Measure

We will show that for fixed pole locations, the product $gG$ of the integrator gains is an approximate measure of the SNR performance of the double-loop modulator. The approximation lies in assuming that the 1-b quantizer $Q$ can be viewed as an independent (not necessarily white) noise source. Although this assumption is not valid and can well be misleading [9], we use it as a guiding line here. It is readily shown that the linearized transfer function between the modulator input and output, assuming no quantization noise, is given by

$$\frac{Y(z)}{X(z)} = \frac{gGx^{-1}}{(\alpha-bg)\beta z^{-2}+(GBg+bg-\alpha-\beta)z^{-1}+1} \tag{7}$$

whereas the transfer function between the quantization noise source $E$ and the modulator output, assuming no modulator input, is given by

$$\frac{Y(z)}{E(z)} = \frac{(1-\alpha z^{-1})(1-\beta z^{-1})}{(\alpha-bg)\beta z^{-2}+(GBg+bg-\alpha-\beta)z^{-1}+1}. \tag{8}$$

The noise suppression relative to the signal filtering is thus given by

$$\frac{gGz^{-1}}{(1-\alpha z^{-1})(1-\beta z^{-1})} \tag{9}$$

which for fixed integrator poles is determined by the product $gG$.

### 4.2 Tone Suppression

The choice of integrator poles is dictated by the rapidity with which unwanted tones are required to be suppressed. The temporal magnification of initial differences is exponential, and intuitively, moving the poles further outside of the unit circle leads to faster tone suppression. It is reasonable, but by no means required, to take the two integrator poles equal,

$\alpha = \beta$; this choice treats perturbations of the two integrators states equally.

To get an idea of the persistence time of tones, let us compare two modulators with their poles on and outside of the unit circle, respectively. Let us assume that for a certain initial state $(U_0, V_0)$ and constant input, a tone exists in the non-chaotic modulator. Very approximately, the quantizer inputs in the two modulators will differ by $U_0(\alpha^n - 1)$ at time $n$, and the difference will at some point cause the quantizer input to have different signs in the two modulators. Once a modulator output bit is flipped in the chaotic modulator compared to the nonchaotic one, the nonlinear folding of the quantizer takes effect, and any simple oscillations are broken. This effect will tend to occur when the quantizer input in the non-chaotic modulator assumes a small value $U_{\text{small}}$. We can therefore estimate the tone persistence time $n_{\text{time}}$ from

$$\alpha^{n_{\text{tone}}} \approx 1 + \left|\frac{U_{\text{small}}}{U_0}\right|. \tag{10}$$

In normal applications, $\alpha$ is close to 1 and $U_{\text{small}}/U_0$ is on the average less than one. Using the approximation $\log(1+x) \approx x$ for $x \ll 1$, we obtain from (10) that

$$n_{\text{tone}} \approx \frac{1}{\alpha - 1}\left|\frac{U_{\text{small}}}{U_0}\right| \lesssim \frac{1}{\alpha - 1}. \tag{11}$$

Very roughly, the expected tone persistence time is thus $1/(\alpha - 1)$. As an example, an audio application may have a sampling rate of 44 100 samples/s, in which case a tone suppression time of a few hundred samples may be acceptable. The integrator poles would need to be on the order of 1.01. As a further example, we can return to Fig. 4, which shows a tone persistence time on the order of 100 samples for pole locations of 1.01.

### 4.3. Design of Double-Loop Modulator

The normalized double-loop modulator contains seven design constants, namely, the scaling factors $(\gamma, \phi, B, g)$, the integrator poles $(\alpha, \beta)$, and the largest normalized constant input $\xi_{\max}$ for which the modulator is designed to operate. The largest unnormalized constant input $X_{\max}$ is related to $\xi_{\max}$ by $X_{\max} = B\xi_{\max}$. Our design approach will be to assume that the integrator poles $(\alpha, \beta)$ are first chosen according to the considerations in Section 4.2 and that $\alpha = \beta$.

Assuming that the integrator poles are specified, we have the same five degrees of design freedom left as in [14], [16], and [17]. Three of these degrees are eliminated by imposing the stability constraints

$$U_{\max} = L, \quad V_{\max} = L, \quad B(1 + \xi_{\max}) = L, \tag{12}$$

where $L$ is a specified circuit clipping level, and $U_{\max}$ and $V_{\max}$ are upper bounds on the absolute values of the state variables. Equation (12) ensures that the integrator outputs as well as the output of the input summing node do not exceed the clipping level. The bounds $U_{\max}$ and $V_{\max}$ are obtained from the weak bounding theorem of Section IV and are only valid for initial potentials determined by the potential $P_C$ in the theorem.

The scaling factors can be manipulated in the following way: Letting $U_{\max 0}$ and $V_{\max 0}$ denote upper bounds on the state variables when $\phi = g = 1$, we must have

$$\phi = \frac{L}{V_{\max 0}}, \qquad g = \frac{L}{\phi U_{\max 0}} = \frac{V_{\max 0}}{U_{\max 0}}, \tag{13}$$

in order to achieve $U_{\max} = L$ and $V_{\max} = L$ when the scaling factors $\phi$ and $g$ are not restricted to unity. Similarly, to satisfy $B(1 + \xi_{\max}) = L$, we must have

$$B = \frac{L}{1 + \xi_{\max}}. \tag{14}$$

Using (1), we then find that

$$G = \frac{\phi}{B} = \frac{1 + \xi_{\max}}{V_{\max 0}} \tag{15}$$

and thus

$$gG = \frac{1 + \xi_{\max}}{U_{\max 0}}. \tag{16}$$

Having used the poles $(\alpha, \beta)$ to suppress tones and the parameters $\phi$, $g$, and $B$ to ensure practical stability, we will use $\gamma$ and $\xi_{\max}$ to optimize the SNR measure $gG$. For a given maximal normalized input $\xi_{\max}$, we must thus choose $\gamma$ to minimize $U_{\max 0}$. For the special case of ideal integrators, the optimal $\gamma$ is given by [14] and [17]

$$\gamma = \begin{cases} 1 + \sqrt{\frac{2}{1-\xi_{\max}}} & \text{for } 0 \le \xi_{\max} \le \sqrt{5} - 2 \\ 1 + \frac{2}{1+\xi_{\max}} & \text{for } \sqrt{5} - 2 < \xi_{\max} < 1. \end{cases} \tag{17}$$

In general, the optimal $\gamma$ is determined numerically as a function of $\xi_{\max}$. The remaining degree of freedom $\xi_{\max}$ controls a tradeoff between the approximate SNR measure $gG$ and the dynamic range of constant inputs specified by

$$X_{\max} = B\xi_{\max} = \frac{L\xi_{\max}}{(1 + \xi_{\max})}.$$

The dynamic range of allowable, un-normalized constant inputs is the range $[-X_{\max}, +X_{\max}]$, which increases monotonically with $\xi_{\max}$. On the other hand, the SNR measure $gG$ typically has a single maximum at some value $\xi_{\max,0}$. The situation is illustrated in Fig. 9, which is drawn for the optimized modulator with poles on the unit circle. A suitable criterion must be established that trades off these two considerations. Our criterion is to choose $\xi_{\max}$ such that $\xi_{\max}$ is greater than $\xi_{\max,0}$ and such that the approximate SNR measure is 10% below its peak value. In this way, the largest normalized input usually becomes a few decibels larger than $\xi_{\max,0}$ at negligible cost in SNR.

## V. Results

We have applied the design technique described in Section 4 to the general double-loop modulator. Table I summarizes the results in a form which is immediately useful to designers. For a given location of integrator poles, the table presents the scaling factors which best trade off the requirements on SNR performance, tone rejection and system stability, as discussed

TABLE I

DESIGN TABLE: Optimized scaling factors as a function of pole locations. The clipping level is denoted by $L$, and the dynamic range for sinusoidal inputs and the safety factor are abbreviated by DR and SF, respectively. The peak SNR and DR numbers are valid for sinusoidal inputs at an oversampling ratio of 128.

| $\alpha$=$\beta$ | $g$ | $G$ | $b/L$ | $B/L$ | $X_{\max}$ | $\gamma$ | Peak SNR (dB) | DR (dB) | $n_{\text{tone}}$ | SF |
|---|---|---|---|---|---|---|---|---|---|---|
| 1 | 0.53 | 0.64 | 0.49 | 0.66 | 0.51 | 2.33 | 90 | 102 | N/A | N/A |
| 1.002 | 0.53 | 0.64 | 0.50 | 0.66 | 0.51 | 2.34 | 90 | 101 | 500 | 47 |
| 1.005 | 0.53 | 0.64 | 0.50 | 0.67 | 0.50 | 2.36 | 89 | 99 | 200 | 17 |
| 1.01 | 0.53 | 0.63 | 0.52 | 0.67 | 0.48 | 2.41 | 87 | 94 | 100 | 8.7 |
| 1.02 | 0.53 | 0.63 | 0.53 | 0.68 | 0.46 | 2.50 | 82 | 93 | 50 | 4.3 |
| 1.03 | 0.52 | 0.62 | 0.55 | 0.69 | 0.44 | 2.58 | 76 | 91 | 33 | 2.9 |
| 1.05 | 0.52 | 0.60 | 0.59 | 0.72 | 0.39 | 2.76 | 67 | 82 | 20 | 1.8 |
| 1.07 | 0.51 | 0.58 | 0.64 | 0.74 | 0.35 | 2.95 | 60 | 74 | 10 | 1.4 |

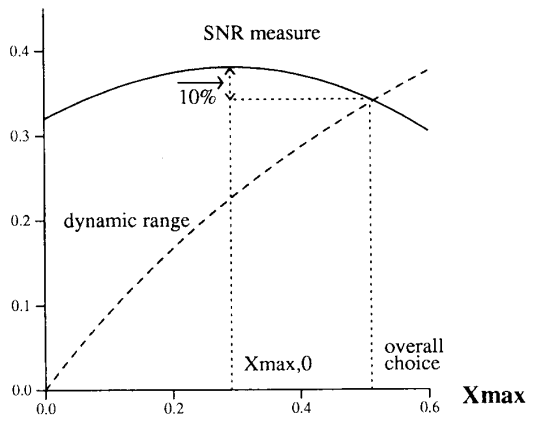


Fig. 9. Tradeoff between approximate SNR measure and dynamic range of constant inputs as a function of normalized constant input.

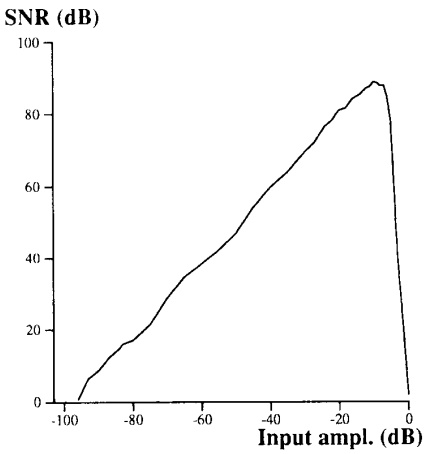


Fig. 10. SNR versus sinusoidal input amplitude for the optimized modulator with poles at 1.005.

previously. The table also shows four parameters relating to the requirements.

- The peak SNR observed in a simulation with sinusoidal inputs of varying amplitudes. Sinusoidal inputs can be considered more realistic than constant inputs, and the application of sinusoidal inputs serves to confirm the design which was carried out for constant inputs. An example of an SNR curve is shown in Fig. 10; the figure is drawn for the optimized double-loop modulator with $\alpha = \beta = 1.005$ and an OSR of 128. The horizontal axis shows the input amplitude in dB relative to an amplitude of 1. A $\text{sinc}^3$ decimation filter was used to remove the high-frequency quantization noise. The input and output conditions were thus identical to those used in [14] and [17].
- The dynamic range of sinusoidal inputs, defined as the range of sinusoidal input amplitudes over which the SNR is at least 0 dB. The dynamic range is measured in decibels and has little connection with the dynamic range of constant inputs specified by $X_{\max}$.
- The estimated tone persistence time $1/(\alpha - 1)$.
- A safety factor relating to system stability. Referring to the potential map in Fig. 11 and to the weak bounding theorem, the safety factor is the ratio $P_C/P_B$, that is, the ratio between the potential at which the upper bound on the potential crosses the 45° line for the last time, and the upper bound on the absolute value of $U$ derived by the bounding technique described in Section III. The safety factor is a measure of the size of the perturbations that would be required to throw a chaotic modulator designed according to our technique into either system instability or clipping. The potential plot in Fig. 11 is the negative potential map for the optimized modulator with its poles at $\alpha = \beta = 1.005$; note the logarithmic axes. The safety factors reported in Table I are the smallest of the safety factors for the positive and negative potential maps.

Note that the peak SNR and the dynamic range of sinusoidal inputs both depend on the OSR used in the sinusoidal input simulation. These numbers should therefore only be taken as examples, and should be replaced by more realistic simulations for any specific application. The other numbers in the table are independent of the OSR.

Note also that the design results for $\alpha = \beta = 1$ differ slightly from the results presented in [14], [16], and [17]. This is exclusively due to the introduction of an objective choice of $\xi_{\max}$ as stated in Section 4.3.

Table I shows that the optimized scaling factors are not very sensitive to changes in pole locations up to $\alpha = \beta = 1.005$. As the poles are moved further outside of the unit circle and into the chaotic regime, the simulated dynamic range and peak SNR decrease more rapidly. Depending on the application, a reasonable design choice might be the optimized modulators with poles at 1.005 or 1.01 that have tone rejection times on

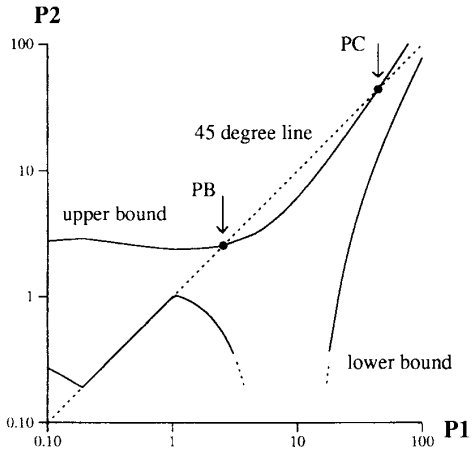


Fig. 11. Log-log plot of the negative potential map for the optimized chaotic modulator with poles at 1.005. The safety factor for the map is defined as the ratio $P_C/P_B$.

the order of 100–200 samples and are not more than 1 b (6 dB) inferior to the optimized modulator with ideal integrators.

The table also shows that the optimal value of the normalized internal feedback factor $\gamma$ increases as the poles move outside of the unit circle. Intuitively, stronger internal feedback is needed for the same degree of stability as the poles are moved outside of the unit circle and the potential for instability increases.

According to the table, the ratio between the tone rejection time and the safety factor is approximately constant at 10–12, indicating that the safety factor decreases approximately as $1/(\alpha - 1)$. Safety factors less than one are impossible, as the conditions of the weak bounding theorem would be violated.

Our design technique breaks down when no potentials can be found for which the weak bounding theorem of Section III holds; this occurs at pole locations of approximately $\alpha = \beta = 1.08$ and is caused by condition 2c of the weak bounding theorem. Simulations indicate that modulators with pole moduli somewhat greater than 1.08 do not behave qualitatively differently than the optimized modulators in Table I. The breakdown is therefore due to inherent limitations in the bounding technique.

## VI. Conclusions

Like other authors [11]–[14], we have argued that chaos may be used constructively to reduce or eliminate disturbing tones in the output of $\Sigma\Delta$ modulators. We have quantified the idea specifically for the general double-loop modulator with constant inputs, and we have derived a semi-analytical method to optimize a tradeoff between tone suppression, SNR performance, and dynamic range. Our results are directly applicable to design of double-loop modulators, which are important practical circuits. However, a circuit designer interested in applying the results should simulate the effect of circuit nonidealities such as finite op–amp gain, which are likely to be dominant in any particular application.

The presented optimization process can potentially be improved in two ways. First, the employed measures of SNR performance and tone persistence are both quite approximate. Second, given better measures, the integrator poles locations could be optimized individually; for instance, it might be advantageous to set $\beta > \alpha \geq 1$ as the noise shaping characteristic tends to depend more critically on integrators further into the loop than on integrators towards the input summing node [14]. On the other hand, it appears difficult to improve upon the state variable bounds. Future research may also be directed towards exploiting chaos in higher order $\Sigma\Delta$ modulators. Although the presented bounding technique relies heavily on the state space being 2-D, it is possible that similar ideas can be applied to higher-order modulators. In any case, it is important to investigate whether higher order modulators are as susceptible to tones as lower order ones and whether the SNR penalty for introducing chaos is indeed a decreasing function of the order as suggested in [12].

Finally, it would be interesting to investigate the utility of chaotic behavior in error diffusion coders for image halftoning. Error diffusion coders are essentially the 2-D analog of $\Sigma\Delta$ modulators. It appears that objectionable artificial patterns in halftoned images could be suppressed through the introduction of chaos. This approach could be easier to implement than dithering, and local average values could be preserved by putting one modulator pole at dc. However, the resulting stability problem appears quite difficult to solve.

## Acknowledgment

The author gratefully acknowledges the contributions of Prof. Zakhor to previous work that inspired the present paper. The simulator used to obtain SNR's for sinusoidal inputs was written by M. Mar.

## References

[1] R. N. Madan, Guest Ed., "Special issue on Chua's circuit: A paradigm for chaos (Part 1)," *J. Circ., Syst. Comp.*, vol. 3, Mar. 1993.
[2] ——, "Special issue on Chua's circuit: A paradigm for chaos (Part 2)," *J. Circ., Syst. Comp.*, vol. 3, June 1993.
[3] J. C. Candy and G. C. T. (Eds.), *Oversampling Delta-Sigma Converters*. New York: IEEE, 1991.
[4] H. Inose and Y. Yasuda, "A unity feedback coding method by negative feedback," *Proc. IEEE*, vol. 51, pp. 1524–1535, Nov. 1963.
[5] R. Devaney, *An Introduction to Chaotic Dynamical Systems*. Redwood City, CA: Addison-Wesley, 1989.
[6] O. Feely and L. O. Chua, "The effect of integrator leak in $\Sigma - \Delta$ modulation," *IEEE Trans. Circuits Syst.*, vol. 38, pp. 1293–1305, Nov. 1991.
[7] ——, "Nonlinear dynamics of a class of analog-to-digital converters," *Int. J. Bifurcation Chaos*, vol. 2, no. 2, pp. 325–340, 1992.
[8] B. E. Boser and B. A. Wooley, "Quantization error spectrum of $\Sigma\Delta$ modulators," in *Proc. Int. Symp. Circuits Syst.*, 1988.
[9] R. M. Gray, "Oversampled Sigma-Delta modulation," *IEEE Trans. Comm.*, vol. COM-35, pp. 481–488, May 1987.
[10] S. R. Norsworthy, "Effective dithering of Sigma-Delta modulators," in *Proc. Int. Symp. Circuits Syst.*, May 1992, pp. 1304–1307.
[11] J. Bulzacchelli, "Chaos in oversampled analog-to-digital converters," Area Exam Rep., MIT, Apr. 1992.
[12] R. Schreier, "Destabilizing limit-cycles in Delta-Sigma modulators with chaos," in *Proc. Int. Symp. Circuits Syst.*, May 1993.
[13] M. Motamed, A. Zakhor, and S. Sanders, "Tones, saturation and SNR in double loop $\Sigma\Delta$ modulators," in *Proc. Int. Symp. Circuits Syst.*, May 1993.
[14] S. Hein and A. Zakhor, *Sigma Delta Modulators: Nonlinear Decoding Algorithms and Stability Analysis*. Boston: Kluwer Academic, 1993.

[15] J. C. Candy, "A use of double integration in Sigma-Delta modulation," *IEEE Trans. Comm.*, vol. COM-33, pp. 249–258, Mar. 1985.
[16] S. Hein and A. Zakhor, "Stability and scaling of double loop Sigma Delta modulators," in *Proc. Int. Symp. Circuits Syst.* (San Diego, CA), May 1992.
[17] ——, "On the stability of Sigma Delta modulators," *IEEE Trans. Signal Processing*, vol. 41, no. 7, pp. 2322–2348, July 1993.
[18] H. Wang, "A geometric view of ΣΔ modulations," *IEEE Trans. Circuits Syst., Part II: Analog and Digital Sig. Processing*, vol. 39, pp. 402–405, June 1992.
[19] S. C. Pinault and P. V. Lopresti, "On the behavior of the double loop Sigma Delta modulator," preprint, 1992.
[20] T. S. Parker and L. O. Chua, "Chaos: A tutorial for engineers," *Proc. IEEE*, vol. 75, pp. 982–1008, Aug. 1987.
[21] O. C. Feely, "An analytical study of the nonlinear dynamics of Sigma-Delta analog-to-digital conversion," Ph.D. thesis, Univ. Calif. Berkeley, May 1992.

**Søren Hein** (S'88–M'93) received the M.Sc. degree in electrical engineering from the Technical University of Denmark in January 1989 and the Ph.D. degree in electrical engineering from the University of California at Berkeley in June 1992.

Since October 1992, he has worked for Siemens Corporate Research and Development in München, Germany. His current research interests include algorithmic aspects of oversampled A/D conversion and halftoning, signal reconstruction, band-limited extrapolation, and signal and image processing for medical and other applications. He has also worked on error-correction coding for satellite communication.

At Berkeley, Dr. Hein received the Eliahu Jury Award for outstanding research in the area of systems, communications, control, or signal processing in 1992 as well as the Outstanding Graduate Student Instructor Award in 1992.